

Bias dependent subband edges and the 0.7 conductance anomaly

Anders Kristensen[†] and Henrik Bruus[‡]

[†]Mikroelektronik Centret, Build. 345, Technical University of Denmark, DK-2800 Lyngby, Denmark

[‡]Niels Bohr Institute, Ørsted Laboratory, Universitetsparken 5, DK-2100 Copenhagen, Denmark

Accepted for publication in *Physica Scripta* (2002), (*Proc. 19th Nordic Semiconductor Meeting, 2001*)

PACS Ref: 73.61.-r, 73.23.-b, 73.23.Ad

Abstract

The 0.7 ($2e^2/h$) conductance anomaly is studied in strongly confined, etched GaAs/GaAlAs quantum point contacts by measuring the differential conductance G as a function of source-drain bias V_{sd} and gate-source bias V_{gs} as well as a function of temperature. In the V_{gs} - V_{sd} plane we use a grayscale plot of the transconductance dG/dV_{gs} to map out the bias dependent transitions between the normal and anomalous conductance plateaus. Any given transition is interpreted as arising when the bias controlled chemical potential μ_d (μ_s) of the drain (source) reservoir crosses a subband edge ε_α in the point contact. From the grayscale plot we extract the constant normal subband edges $\varepsilon_0, \varepsilon_1, \dots$ and most notably the bias dependent anomalous subband edge $\varepsilon'_0(\mu_d)$ split off from ε_0 . We show by applying a finite-bias version of the recently proposed BCF model, how the bias dependence of the anomalous subband edge is the key to analyze various experimental observations related to the 0.7 anomaly.

1. Introduction

The quantized conductance of a narrow quantum point contact with subband edges ε_α connecting the source and drain reservoirs of two-dimensional electron gas (2DEG) was discovered in 1988 by van Wees et al. [1] and Wharam et al. [2]. The quantization of the conductance in units of the spin degenerate conductance quantum, $G_2 = 2e^2/h$, can be explained within a single-particle picture in terms of the Landauer-Büttiker formalism involving the transmission coefficients $\mathcal{T}[\varepsilon, \varepsilon_\alpha]$ of the subbands α in the constriction. For a review see Ref. [3].

The observation by Thomas et al. [4], later confirmed by others [5]–[14] of the so-called 0.7 conductance anomaly is possibly the first experimental indication of many-body phenomena in semiconductor quantum point contacts and wires. At zero source-drain bias, V_{sd} , the 0.7 anomaly is a suppression of the differential conductance, $G = dI/dV_{sd}$, at the low-density end of the first quantized conductance plateau, $G = 1.0 G_2$. It appears as a shoulder-like structure around $G = 0.7 G_2$, which sometimes develops into a conductance plateau, that becomes more pronounced as the temperature is raised. At high temperatures the conductance suppression exhibits activated behavior as function of temperature [7, 10], and a density-dependent activation temperature, T_A , or energy, $\Delta = kT_A$ can be extracted. At finite V_{sd} , the 0.7 anomaly evolves into a well-defined conductance plateau at $G = 0.85 G_2$ [15, 16] and, as V_{sd} is increased further, into another plateau at $G = 1.4 G_2$ [10], see also Fig. 1.

In addition to the differential conductance measurements, the 0.7 anomaly has also been studied using other experimental methods: the series conductance of two point contacts [17], suppression of shot-noise [18], thermopower measurements [19] and acousto-electric currents induced

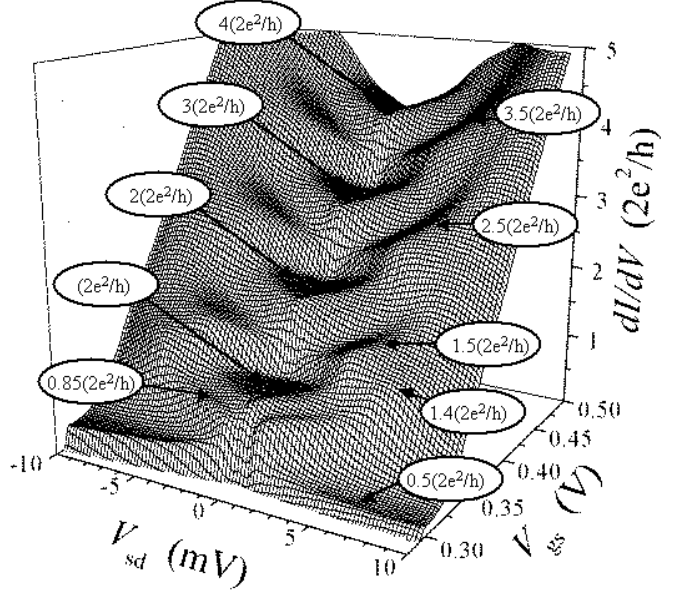


Figure 1: Measurement of the differential conductance $G = dI/dV_{sd}$ versus gate-source voltage V_{gs} and source-drain bias voltage V_{sd} . The data are taken at $T = 0.3$ K on sample A in Ref. [10]. Normal integer conductance plateaus, $G = n 2e^2/h$, are seen at $V_{sd} = 0$ mV and the well-known half-plateaus, $G = (n + \frac{1}{2}) 2e^2/h$, at $V_{sd} \sim \pm 3$ mV. In addition anomalous plateaus appear with $G = 0.85 2e^2/h$ and $G = 1.4 2e^2/h$ at $V_{sd} \sim \pm 2$ mV and $\sim \pm 7$ mV, respectively.

by surface acoustic waves (SAW) [20].

Recently Bruus, Cheianov, and Flensberg proposed a model [21], henceforth denoted the BCF model, which provides a unifying explanation of different types of experiments related to the 0.7 anomaly: the anomalous effects are interpreted in terms of anomalous, bias dependent 1D subband edges, split off from each normal 1D subband. In our opinion, further investigations of these anomalous subband edges is the key to a deeper understanding of the 0.7 structure. This point of view will be emphasized in this paper by comparing the results of a number of experiments with model calculations based solely on the input from one experiment: the low-temperature determination of the anomalous subband edge $\varepsilon'(\mu_d)$.

2. The bias dependent subband edge $\varepsilon'(\mu_d)$

The experimental data presented in this paper are all obtained from sample A described in detail in our previous paper [10], a shallow etched topgated GaAs/GaAlAs

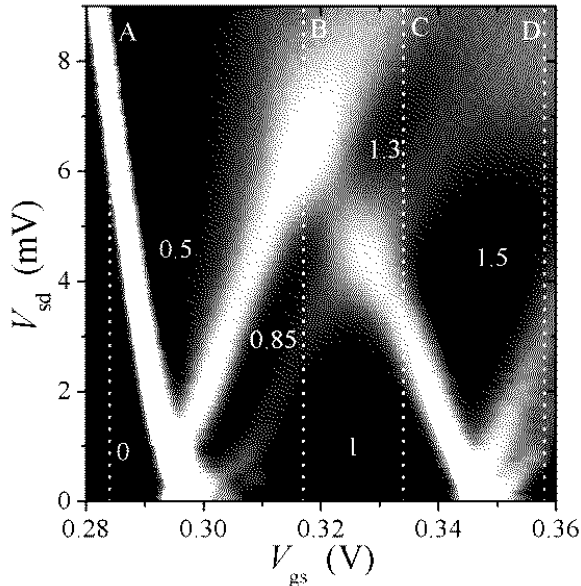


Figure 2: Part of the experimental data from Fig. 1 presented as a grayscale plot of the transconductance, $dG/dV_{gs}(V_{gs}, V_{sd})$. Black corresponds to zero transconductance, i.e. to plateaus in the differential conductance, $G = dI/dV_{sd}$. White corresponds to high transconductance. The bright lines in the plot therefore indicate the positions (V_{gs}, V_{sd}) of transitions between the various conductance plateaus. The numbers indicate the value of G in units of $2e^2/h$ on the various plateaus. The dashed vertical lines A–D indicate sweeps in V_{sd} at four fixed values of V_{gs} ; see Sec. 5.

quantum point contact 200 nm wide opening (determined lithographically). An overview of the observed conductance quantization is presented in the surface plot Fig. 1, where the differential conductance $G = dI/dV_{sd}$ is plotted versus gate-source voltage V_{gs} and source-drain bias voltage V_{sd} . The data are taken at $T = 0.3$ K. Normal integer conductance plateaus [1, 2], $G = n G_2$, are seen at $V_{sd} = 0$ mV and the well-known half-plateaus [22, 23], $G = (n + \frac{1}{2}) G_2$, at $V_{sd} \sim \pm 3$ mV. In addition anomalous plateaus [10, 15, 16] appear with $G = 0.85 G_2$ and $G = 1.4 G_2$ at $V_{sd} \sim \pm 2$ mV and $\sim \pm 7$ mV, respectively. A thorough analysis of this data, including e.g. electrostatic self-gating effects, is given in Sec. IV of Ref. [10]. In this paper we focus on the anomalous $G = 0.85 G_2$ and $1.4 G_2$ plateaus.

The conductance anomalies appear very clearly in the transconductance, dG/dV_{gs} , which is calculated by numerical differentiation of the data in Fig. 1. In Fig. 2 it is represented as a grayscale plot in the V_{gs} – V_{sd} plane. Plateau regions, e.g. regions with small transconductance appear as black regions bounded by bright, high transconductance transition regions. The clearest feature of the plot is the usual straight but slanted white transition lines surrounding the integer and half-integer plateaus $G = 0.0, 0.5, 1.0$, and $1.5 G_2$ [16]. But the feature of interest in this paper is the weaker gray transition line dividing the $G = 0.85 G_2$ plateau from the $G = 1.0 G_2$ plateau and further on dividing the $G = 1.4 G_2$ plateau from the $G = 1.5 G_2$ plateau.

The central point in our analysis is that we interpret all transitions between conductance plateaus, including the anomalous ones, as arising when the chemical potential μ_s of the source or μ_d of the drain reservoir crosses the subband edges ε_α in the point contact.

In the conventional half-plateau analysis [22, 23] the straight white transition lines between the conductance plateaus $G = 0.0, 0.5, 1.0$, and $1.5 G_2$ are explained as follows. For $V_{sd} = 0$ mV the $G = 1.0 G_2$ plateau begins at $V_{gs} = V_{gs}^a$ and ends at $V_{gs} = V_{gs}^b$,

$$V_{gs}^a = 292 \text{ mV}, \quad V_{gs}^b = 347 \text{ mV}. \quad (1)$$

Each value of V_{gs} results in a certain average chemical potential $\mu_0(V_{gs})$. We shall assume a simple linear function with coefficients α and β to be determined shortly,

$$\mu_0(V_{gs}) = \alpha V_{gs} + \beta. \quad (2)$$

In energy space the $G = 1.0 G_2$ plateau occurs when the chemical potential lies between the subband edges ε_0 and ε_1 , and we have

$$\mu_0(V_{gs}^a) \equiv \varepsilon_0, \quad \mu_0(V_{gs}^b) \equiv \varepsilon_1. \quad (3)$$

As finite source-drain bias is applied the chemical potentials μ_s and μ_d of the source and drain reservoirs are shifted away from their average value μ_0 according to

$$\mu_d(V_{gs}, V_{sd}) \equiv \mu_0(V_{gs}) - \frac{1}{2} e V_{sd}, \quad (4)$$

$$\mu_s(V_{gs}, V_{sd}) \equiv \mu_0(V_{gs}) + \frac{1}{2} e V_{sd}. \quad (5)$$

In the following we take $V_{sd} > 0$ and denote the reservoir with the lower chemical potential the drain reservoir. A transition from one plateau to another happens when μ_d aligns with a subband edge ε_n or when μ_s aligns with ε_m ,

$$\mu_d = \varepsilon_n \Rightarrow V_{sd} = \frac{2}{e}(\beta - \varepsilon_n + \alpha V_{gs}), \quad (6)$$

$$\mu_s = \varepsilon_m \Rightarrow V_{sd} = \frac{2}{e}(\varepsilon_m - \beta - \alpha V_{gs}). \quad (7)$$

Clearly, transition lines with positive (negative) slope in the grayscale plot occur when the chemical potential in the drain (source) crosses a subband edge ε_n (ε_m). We can immediately conclude that the anomalous transition line with its positive slope involves the splitting off of the anomalous subband edge ε'_0 from the normal subband edge ε_0 when the drain chemical potential μ_d crosses ε_0 , while the subband remains unchanged as the source chemical potential μ_s crosses ε_0 .

There is one fundamental difference between the normal and the anomalous plateaus. At finite bias normal spin-degenerate plateaus occurs in intervals of $1/2 G_2$, while spin polarized plateaus occurs in intervals of $1/4 G_2$. The anomalous one involves units of $1/8 G_2$, e.g. $0.85 \approx 1.0 - 1/8$, and $1.4 \approx 1.5 - 1/8$. This is explained in Sec. 3 by the BCF model, but we summarize the conditions for plateau formation now. The width of a transition is governed by a parameter T^* being a combination of the actual temperature T and the tunneling parameter T_t . A normal plateau occurs when the chemical potentials μ_s and μ_d are

more than a few times kT^* away from subband edges ε_α . According to the BCF model an anomalous plateau occur when the chemical potential μ_d of the drain is less than a few times kT^* away from an anomalous subband edge $\varepsilon'_\alpha(\mu_d)$. In short, we have the following conditions for plateau formation:

$$\text{normal plateau : } |\mu_{s,d} - \varepsilon_\alpha| > 4kT^*, \quad (8)$$

$$\text{anomalous plateau : } |\mu_d - \varepsilon'_\alpha(\mu_d)| < 4kT^*. \quad (9)$$

In Ref. [21] the function name Δ was introduced for the energy difference in Eq. (9), and when it is positive it can be interpreted as the Fermi energy of the anomalous subband, e.g. for ε'_0

$$\Delta(\mu_d) \equiv \mu_d - \varepsilon'_n(\mu_d). \quad (10)$$

We are now ready to determine the explicit expressions for the subband edges based on the data in Fig. 2. The normal transition lines $\mu_s = \varepsilon_1$ and $\mu_d = \varepsilon_0$ cross at the point $(V_{gs}, V_{sd}) = (320 \text{ mV}, 6.5 \text{ mV})$. Adding Eqs. (7) and (6) after insertion of these numbers leads to $\varepsilon_1 - \varepsilon_0 = eV_{sd} = 6.5 \text{ meV}$. If we choose the energy zero to be at ε_0 we end up with the following normal subband edges.

$$\varepsilon_0 = 0.0 \text{ meV}, \quad (11)$$

$$\varepsilon_1 = 6.5 \text{ meV}. \quad (12)$$

Combining Eqs. (1), (2), (3), (11) and (12) leads to

$$\mu_0(V_{gs}) = 0.13 V_{gs} - 38.35 \text{ meV}. \quad (13)$$

Concerning the anomalous $G = 0.85 G_2$ plateau in Fig. 2 we note that the white transition lines on either side of it are almost parallel and separated by $\Delta V_{gs} \approx 15 \text{ mV}$. Using Eq. (13) we can deduce the width in energy space of the anomalous plateau to be $\sim 2 \text{ meV}$. Combined with Eq. (9) we arrive at

$$\varepsilon'_0(\mu_d) \begin{cases} \approx \mu_d, & \text{for } 0 < \mu_d < 2 \text{ meV}, \\ = 0, & \text{otherwise.} \end{cases} \quad (14)$$

The three subband edges ε_0 , $\varepsilon'_0(\mu_d)$, and ε_1 are the main input to the BCF model calculations used to analyze all our experiments in the rest of the paper.

3. The BCF model at finite bias

The central idea in the BCF model is that the degeneracy of the first, but in principle any, two-fold degenerate subband, is lifted as the chemical potential of the drain crosses the subband edge ε_0 . One of the resulting non-degenerate subband edges, the normal one, remains at ε_0 while the other, the anomalous $\varepsilon'_0(\mu_d)$, follows μ_d such that the deviation $\Delta(\mu_d) = \mu_d - \varepsilon'_\alpha(\mu_d)$ is a power law [21]. All the phenomenology of the 0.7 anomaly is contained in this power law that leads to the all important tendency of the anomalous subband edge to pin to μ_d . We will not engage in a discussion concerning the foundation of this model, but just use it as a phenomenological input to the Landauer-Büttiker formalism, and from this obtain a unified interpretation of our experimental results.

As summarized in Eq. (14) the first anomalous conductance plateau of sample A is determined experimentally

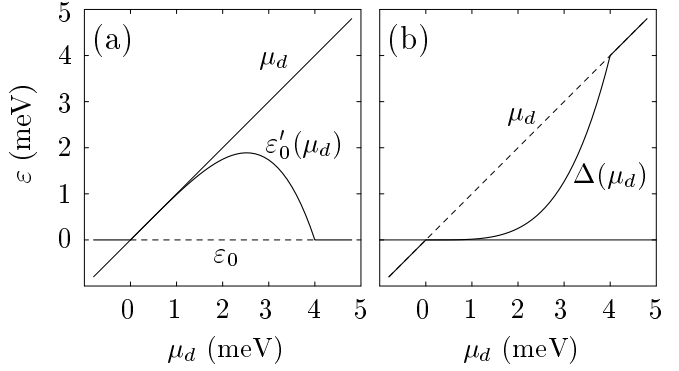


Figure 3: (a) The position of the anomalous subband edge $\varepsilon'_0(\mu_d)$ given by Eq. (15) with $n = 3$ and $\mu^* = 4.0 \text{ meV}$ as in Secs. 4 and 5. (b) Graph of the anomalous subband Fermi energy $\Delta(\mu_d)$ Eq. (10) exhibiting the power law behavior for μ_d near 0 mV required by the BCF model.

to occur for $0 < \mu_d < 2 \text{ meV}$. In this interval we must demand that $\varepsilon'_0(\mu_d) \approx \mu_d$. If we also assume the power law behavior of the BCF model, we can fulfill both these requirements by the following simple function

$$\varepsilon'_0(\mu_d) = \begin{cases} \mu_d(1 - \mu_d/\mu^*)^n, & \text{for } 0 < \mu_d < \mu^*, \\ 0, & \text{otherwise.} \end{cases} \quad (15)$$

In Fig. 3 are depicted the graphs of $\varepsilon'_0(\mu_d)$ and $\Delta(\mu_d)$ with the choice of parameters $n = 3$ and $\mu^* = 4.0 \text{ meV}$ as described in Sec. 4.

To be able to analyze Fig. 2 we extend the BCF model, treated so far only in the linear response regime, by combining it with the standard half-plateau theory [23] based on the finite bias version of the Landauer-Büttiker formula. Crucial ingredients in this treatment are the subband edges ε_α of the point contact, $\alpha = 0, 0', 1, \dots$, and the energy dependent transmission coefficients $\mathcal{T}[\varepsilon, \varepsilon_\alpha]$. In practice these coefficients cannot be determined completely, and here we restrict our treatment to two simple examples, the perfect adiabatic transmission $\mathcal{T}_{ad}[\varepsilon, \varepsilon_\alpha]$ and the slightly more realistic case [24] of non-adiabatic tunneling smeared transmission $\mathcal{T}_{tn}[\varepsilon, \varepsilon_\alpha]$:

$$\mathcal{T}_{ad}[\varepsilon, \varepsilon_\alpha(\mu_d)] = \Theta[\varepsilon - \varepsilon_\alpha(\mu_d)], \quad (16)$$

$$\mathcal{T}_{tn}[\varepsilon, \varepsilon_\alpha(\mu_d)] = \frac{1}{\exp[(\varepsilon_\alpha(\mu_d) - \varepsilon)/kT_t] + 1}, \quad (17)$$

where $\Theta[x]$ is the usual step function, and T_t is a parameter (here written as a characteristic temperature) describing the degree of smearing of the transmission coefficient due to reflection above and tunneling below the subband edge.

The current $I(V_{sd}, V_{gs}, T)$ at finite bias is calculated in terms of the transmission coefficients, the degeneracy factor $\lambda_\alpha = 1, 2$ of subband ε_α , and the Fermi-Dirac distribution function $f(\varepsilon, \mu_{s/d}, T)$ of the source and drain reservoirs as

$$I[\mu_s(V_{gs}, V_{sd}), \mu_d(V_{gs}, V_{sd}), T] \quad (18)$$

$$= \frac{e}{h} \sum_\alpha \lambda_\alpha \int_{-\infty}^{\infty} d\varepsilon \mathcal{T}[\varepsilon, \varepsilon_\alpha(\mu_d)] [f(\varepsilon, \mu_s, T) - f(\varepsilon, \mu_d, T)].$$

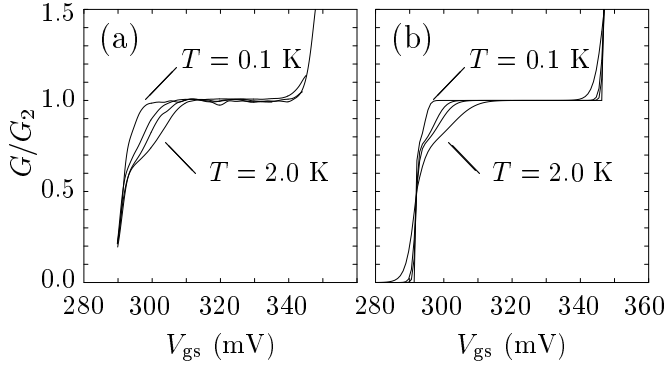


Figure 4: (a) The measured zero-bias differential conductance $G(V_{\text{gs}})$ exhibiting a strengthening of the 0.7 anomaly as the temperatures is raised from 0.1 K, through 0.5 K and 0.8 K, ending at 2.0 K. (b) BCF model calculation of G_{ad} Eq. (20) for $T = 0.1, 0.5, 0.8,$ and 2.0 K using the parameter values given in Sec. 6. Note the fair agreement between experiment and theory even in the simple case of adiabatic transmission.

Generally the current is found from Eq. (18) by numerical integration. However, since $\int dx (e^x + 1)^{-1} = x - \ln(e^x + 1)$, simple analytical results can be obtained when the adiabatic transmission coefficient \mathcal{T}_{ad} of Eq. (16) is used. In the following we shall use \mathcal{T}_{ad} extensively and only in Sec. 6 switch to the non-adiabatic, tunneling smeared transmission coefficient \mathcal{T}_{tn} of Eq. (17).

In the case of adiabatic transmission the finite bias, differential conductance $G_{\text{ad}}(V_{\text{gs}}, V_{\text{sd}}, T) = dI/dV_{\text{sd}}$ is

$$G_{\text{ad}}[\mu_s(V_{\text{gs}}, V_{\text{sd}}), \mu_d(V_{\text{gs}}, V_{\text{sd}}), T] = \frac{G_2}{4} \sum_{\alpha} \lambda_{\alpha} \quad (19)$$

$$\times \left(\frac{1}{1 + \exp\left[\frac{\varepsilon_{\alpha}(\mu_d) - \mu_s}{kT}\right]} + \frac{1}{1 + \exp\left[\frac{\varepsilon_{\alpha}(\mu_d) - \mu_d}{kT}\right]} \right).$$

In the limit of zero temperature the conductance G_{ad} Eq. (19) is seen to increase in units of $(\lambda_{\alpha}/4) G_2$ each time μ_s or μ_d crosses a subband edge ε_{α} . In the standard case, where all subbands two-fold degenerated and all subband edges are constant, the conductance unit is the usual G_2 if $V_{\text{sd}} = 0$, while the half-plateau values $0.5 G_2$ are recovered for finite bias, $V_{\text{sd}} \neq 0$.

Anomalous plateaus can also be obtained from Eq. (19). Assuming the BCF model Eq. (15) the inequality $\varepsilon'_0(\mu_d) < \mu_d \ll kT$ is fulfilled in a finite interval $0 < \mu_d \ll \mu^*$, thus yielding $1/(1 + \exp[(\varepsilon'_0(\mu_d) - \mu_d)/kT]) \approx 1/2$, i.e. half of the zero temperature value. Since in the BCF model the degeneracy of the lowest subband is lifted, we have $\lambda_{0'} = 1$. This means that the conductance on the anomalous plateau is lowered by $1/4 G_2$ if $V_{\text{sd}} = 0$ (where $\mu_s = \mu_d$) and by $1/8 G_2$ if $V_{\text{sd}} \neq 0$ (where $\mu_s \neq \mu_d$). Consequently, in accordance with the measurements, we find at zero bias the anomalous plateau $G = (1 - 1/4) G_2 = 0.75 G_2$, and at finite bias $G = (1 - 1/8) G_2 = 0.875 G_2$ as well as $G = (3/2 - 1/8) G_2 = 1.375 G_2$.

As an example of a full conductance formula involving anomalous plateaus we give the BCF formula for G_{ad} in the zero bias limit where $\mu_s = \mu_d = \mu$. We restrict the for-

mula to the lowest three subbands ε_0 , $\varepsilon'_0(\mu)$, and ε_1 with degeneracies $\lambda_0 = 1$, $\lambda_{0'} = 1$, and $\lambda_1 = 2$, respectively:

$$G_{\text{ad}}(\mu, \mu, T) = G_2 \quad (20)$$

$$\times \left(\frac{1/2}{1 + e^{(\varepsilon_0 - \mu)/kT}} + \frac{1/2}{1 + e^{(\varepsilon'_0(\mu) - \mu)/kT}} + \frac{1}{1 + e^{(\varepsilon_1 - \mu)/kT}} \right),$$

In Fig. 4 is shown a comparison at different temperatures between low-bias experimental measurements on G and BCF model calculations based on Eq. (20). A good qualitative agreement is seen, in particular concerning the strengthening of the 0.7 conductance anomaly as the temperature is increased. In Sec. 6 we give a more detailed analysis of the temperature dependence of the 0.7 conductance anomaly at zero bias.

4. Transconductance in the BCF model

By differentiation of Eq. (19) it is a simple matter to calculate the transconductance dG/dV_{gs} . This can then be used to reproduce the grayscale plot of Fig. 2 theoretically by combining it with the experimentally determined subband edges ε_0 , Eqs. (11), and ε_1 , Eq. (12) as well as the BCF model of the anomalous edge $\varepsilon'_0(\mu_d)$, Eq. (15). For the latter we use the values $n = 3$ and $\mu^* = 4.0$ meV found by visual fitting to the data. The resulting grayscale plot of the transconductance is shown in Fig. 5.

The main features are well reproduced: the straight white lines of the half-plateau model and the gray line with positive slope parallel to the white line forming the right-hand edge of the $G = 0.5 G_2$ plateau. A number of minor features are not reproduced at all, simply due to the omission of certain physical effects in the model.

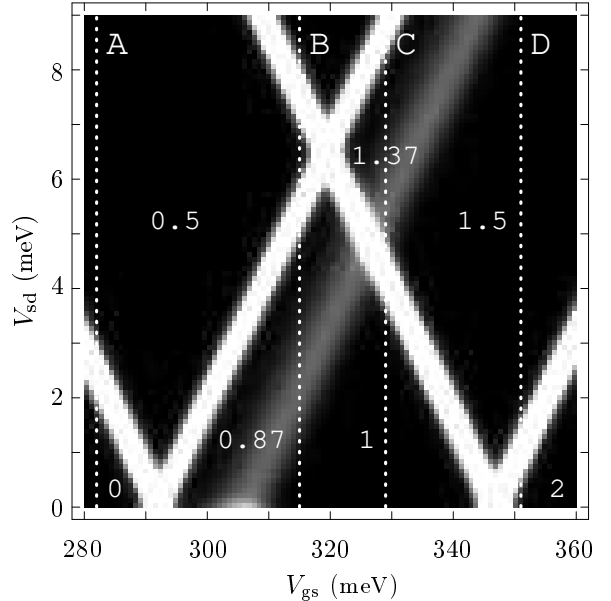


Figure 5: Calculated transconductance dG/dV_{gs} based on the conductance formula Eq. (19), valid in the case of adiabatic transmission, using the BCF model of the anomalous subband edge $\varepsilon'_0(\mu_d)$ Eq. (15) with $n = 3$ and $\mu^* = 4$ meV. To mimic tunneling-induced smearing of the plateaus the temperature is set to 1 K, somewhat higher than the 0.3 K of the actual experiment. The sweeps in V_{sd} along the lines A–D are studied in Sec. 5.

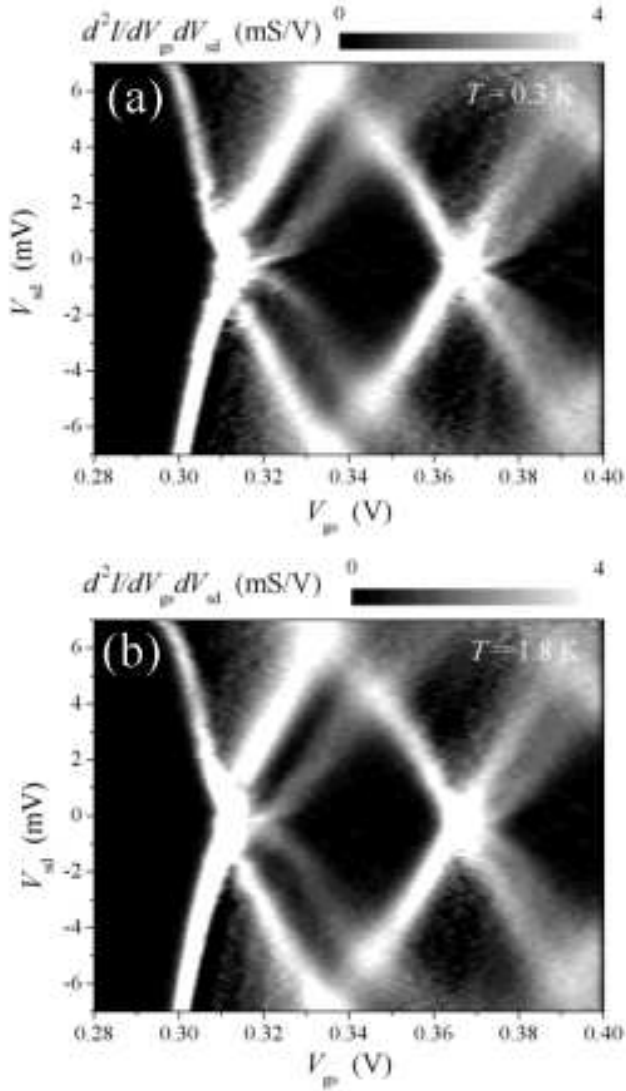


Figure 6: Differential transconductance as in Fig. 2 measured at $T = 0.3$ and 1.8 K. The structures are not changed significantly by changing the temperature by a factor of six.

Firstly, the left border of the experimental $G = 0.5 G_2$ plateau is not quite straight. This is presumably due to Coulomb interaction effects dominating the point contact at the very low densities as it opens up for conduction. Electron interaction was not included in the model.

Secondly, most structures in Fig. 2 tend to be smeared out at high values of V_{sd} . This is probably due to heating of the electron system by applying such high values of the bias voltage. Also, the Fermi energy of the 2DEG reservoirs is 10 meV, and when eV_{sd} at the top of the grayscale plot approaches this value, strong distortions of the system occur. Neither of these two effects are taken into account in the model calculation.

Thirdly, the anomalous 0.85 – 1 transition line is not quite parallel to the white 0.5 – 0.85 transition line in the experiment. This may also be an effect of bias induced heating. As the temperature is increased the width of the anomalous plateau is increased as shown by the zero-bias data in Fig. 4. This would lead to an increased distance between the 0.5 – 0.85 and 0.85 – 1.0 transition line as V_{sd} is

increased. That heating due to the finite bias is important may be deduced from Fig. 6. In this figure are shown two experimental grayscale plots recorded at the two cryostat temperatures 0.3 K and 1.8 K, respectively. The main features of the plots are not changed significantly by the six-fold increase of the temperature. However, except for the 0 – 0.5 transition line, there is the above mentioned tendency of stronger smearing of the transition lines as V_{sd} is increased. Thus heating due to the cryostat temperature is negligible compared to the smearing due to bias induced heating.

Lastly, at low bias the anomalous 0.85 – 1 transition line deviates from a straight line in the experiment: the width of the anomalous plateau shrinks as the bias is lowered. In the model calculation we have used constant values for the parameters μ^* and n in Eq. (15), and therefore we obtained a constant width.

Further studies of all these effects are in progress.

5. G at finite bias, experiments and model

The grayscale plots of the transconductance in Figs. 2 and 5 expose clearly the position of the subband edges but reveals nothing about the value of the conductance at the plateaus. To find the plateau values we go back and study the differential conductance G . In Fig. 7 is shown the graphs of $G(V_{sd})$ obtained from the bias sweeps A–D indicated in the experimental and theoretical grayscale plots Figs. 2 and 5.

The experimental curves of $G(V_{sd})$ in Fig. 7(a) recorded for $V_{gs} = 284, 317, 334,$ and 358 mV shows the appearance of the half-plateaus $0.5, 1.0, 1.5$ and 2.0 , but they are in particular chosen to show the quite well developed anomalous plateau $G = 0.85 G_2$, and the rather smeared anomalous plateau at $G = 1.35 G_2$.

The BCF model calculation of $G(V_{sd})$ in Fig. 7(b) with $V_{gs} = 282, 315, 329,$ and 351 mV reproduces the experimentally observed features fairly well. In particular well developed anomalous plateaus are seen at $G = 0.87$ and $1.37 G_2$.

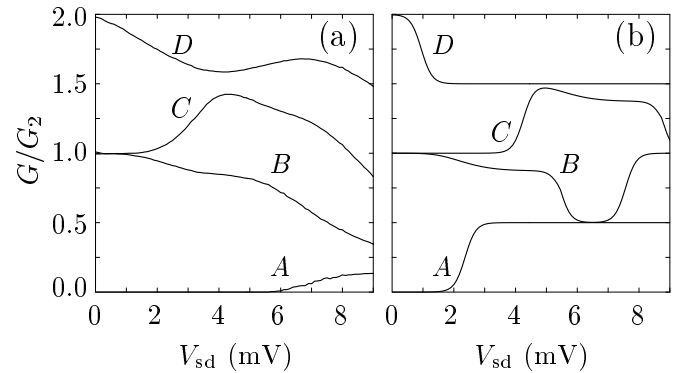


Figure 7: (a) The measured differential conductance $G(V_{sd})$ along the four V_{sd} sweep-lines A–D indicated in Fig. 2 with $T = 0.3$ K. (b) BCF model calculation of $G(V_{sd})$ along the four V_{sd} sweep-lines A–D indicated in Fig. 5 using Eq. (19) with adiabatic transmission \mathcal{T}_{ad} and $T = 1.0$ K.

Naturally, the remarks made in Sec. 4 concerning the deficiencies of the BCF model are also valid here. The experimentally observed bending of the 0–0.5 transition line in the grayscale plot shows up as a large upward shift in V_{sd} of the D–curve in Fig. 7(a) as compared to the D–curve in the model calculation Fig. 7(b). The strong deformation of the spectrum for high bias voltages in the experiment appears as a marked downward bending of the A, B, and C–curve in Fig. 7(a). Finally, we also see the effect of the absence of tunneling in the model calculation: the calculated transitions between plateaus in Fig. 7(b) are much steeper than the observed ones in Fig. 7(a) despite the fact that the temperature in the model is set to 1.0 K, i.e. higher than the 0.3 K of the experiment.

6. Activated conductance suppression at low bias

The fair agreement between experiment and model calculation in Fig. 4 makes a comparison desirable which is more detailed than the simplistic Arrhenius analysis presented in Ref. [10]. As mentioned in the end of Sec. 4 the width of the plateau shrinks as V_{sd} goes to zero. We therefore use the zero bias data in Ref. [10] to fit the values for the parameters n and μ^* in Eq. (15), and we find $n = 1$ and $\mu^* = 8.5$ meV. Due to the exponential factors appearing in the Fermi-Dirac distribution functions it is natural to plot the deviation from perfect quantization as $\ln[1 - G(T)/G_2]$ versus $1/T$. We set $V_{sd} = 0$ mV and focus on the first half of the first plateau by choosing the following four fixed values of the gate–source voltage: $V_{gs} = 305, 310, 315,$ or 320 mV.

In Fig. 8(a) we compare model calculations based on the conduction Eq. (19) for the case of adiabatic transmission \mathcal{T}_{ad} of Eq. (16) in the BCF model and for the case of normal rigid subband edges fixed at ε_0 and ε_1 . We see how the two calculations deviates both for small and large values of $1/T$. The BCF values are systematically higher than the values of the rigid subband edge model.

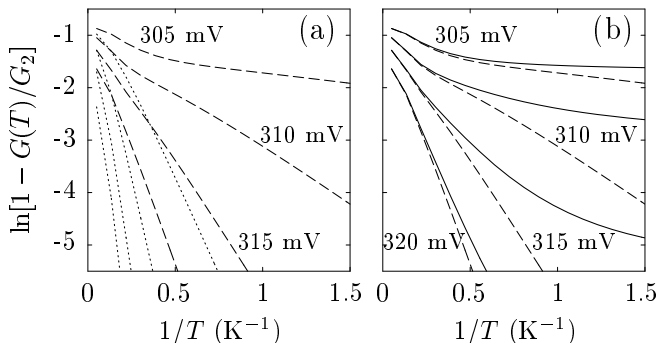


Figure 8: (a) Comparison of the calculated conductance suppression $\ln[1 - G(T)/G_2]$ versus $1/T$ with adiabatic transmission for $V_{gs} = 305, 310, 315,$ and 320 mV in two cases. Dotted lines: normal rigid subband edges, and dashed lines: the anomalous density dependent subband edge, i.e. the BCF-model. (b) The BCF-model as in (a) with adiabatic transmission (dashed lines) compared to the BCF-model with the non-adiabatic tunneling transmission of Eq. (17) (full lines).

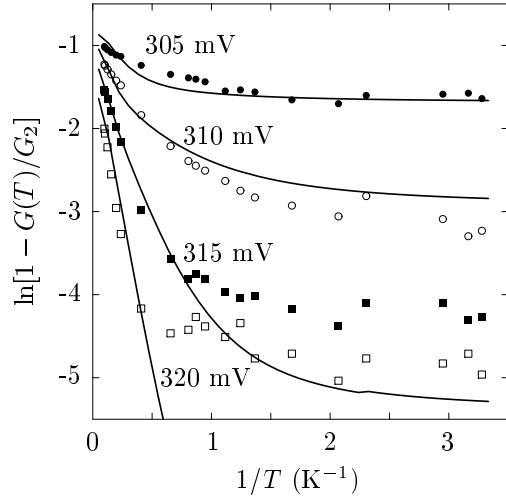


Figure 9: Comparison of experimental data (points) and BCF model calculation (full lines) of the conductance suppression $\ln[1 - G(T)/G_2]$ versus $1/T$ for the gate–source voltages $V_{gs} = 305$ (●), 310 (○), 315 (■), and 320 mV (□). The data are obtained from the same sample as in Figs. 1 and 2. The calculation is performed using the non-adiabatic tunneling transmission \mathcal{T}_{tn} Eq. (17) with the smearing parameter $T_t = 1.1$ K.

In Fig. 8(b) we compare two versions of the BCF model: one, the adiabatic case from Fig. 8(a) using \mathcal{T}_{ad} of Eq. (16), and the other using the non-adiabatic tunneling transmission \mathcal{T}_{tn} of Eq. (17) with $T_t = 1.1$ K. Here we note that in the high temperature regime (small values of $1/T$) the two cases produce identical results: tunneling is not important. However, at temperatures lower than 1 K (large values of $1/T$), substantial deviations occur due to tunneling induced suppression of the conductance: the non-adiabatic point contact is further away from perfect quantization, hence resulting in higher values in the plot.

Finally, in Fig. 9 we compare experimental values of $\ln[1 - G(T)/G_2]$ with the BCF model calculation of Fig. 8(b) including smearing by tunneling. Good agreement is obtained in the high temperature regime in all four cases, while in the low temperature regime (large values of $1/T$) only the most strongly deviating conductance traces are comparing well. It is to be expected that when studying minute deviations from perfect quantization the exact form of $\mathcal{T}[\varepsilon, \varepsilon_\alpha]$ plays an increasingly important role. There is a priori no reason why $\mathcal{T}_{tn}[\varepsilon, \varepsilon_\alpha]$ of Eq. (17) should match the actual transmission function of the sample.

7. Conclusion

In this work we have shown how the experimental determination at finite bias and low temperatures of the three subband edges ε_0 , $\varepsilon'_0(\mu_d)$, and ε_1 can be used as input to the BCF model resulting in model calculations, which can predict the results of other experiments. In particular we have shown this to be the case explicitly for grayscale plot of the transconductance, the finite bias values of the differential conduction $G(V_{sd})$, and of the temperature dependence of the suppression $\ln[1 - G(T)/G_2]$. In all cases the model calculations resulted in fair agreement with the

experiments, and we have thereby demonstrated how the BCF model with the subband edges as input provides a unified way to analyze and understand a wide range of data related to the 0.7 anomaly.

This way of analyzing experiments related to the 0.7 anomaly may be very profitable to apply to the existing data on other experiments than those treated in this paper: the series conductance of two point contacts [17], suppression of shot-noise [18], thermopower measurements [19] and acousto-electric currents induced by surface acoustic waves (SAW) [20]. For the thermopower, a BCF model calculation comparing well with experiments has already been performed successfully [25].

This and previous work has led us to believe that the anomalous subband edges combined with the BCF model may be the key to a deeper understanding of the 0.7 structure. To allow for better analysis along these lines we would therefore like to encourage experimentalists always to measure the subband edges, using e.g. the finite bias transconductance, whenever measuring other effects related to the 0.7 anomaly. Finally, we note that at present the BCF model has no microscopic foundation, and naturally it is highly desirable to derive such a foundation theoretically.

Acknowledgements

This work was supported by the Danish Technical Research Council (grant no. 9701490) and by the Danish Natural Science Research Council (Ole Rømer grant no. 9600548). The GaAs heterostructure used in this investigation was grown at the III-V NANOLAB, Ørsted Laboratory, Niels Bohr Institute, by Claus B. Sørensen.

References

- [1] B.J. van Wees, H. van Houten, C.W.J. Beenakker, J.G. Williamson, L.P. Kouwenhoven, D. van der Marel, and C.T. Foxon, *Phys.Rev.Lett.* **B 60**, 848 (1988).
- [2] D.A. Wharam, T.J. Thornton, R. Newbury, M. Pepper, H. Ahmed, J.E.F. Frost, D.G. Hasko, D.C. Peacock, D.A. Ritchie, and G.A. Jones, *J.Phys.C* **21**, L209 (1988).
- [3] H. Van Houten, C.W.J. Beenakker, and B. van Wees, p. 9 in *Nanostructured Systems*, M. Reed eds., *Semiconductors and Semimetals*, R.K. Williamson, A.C. Beer and R. Weber eds. (Academic Press, 1992).
- [4] K.J. Thomas, J.T. Nicholls, M.Y. Simmons, M. Pepper, D.R. Mace, and D.A. Ritchie, *Phys. Rev. Lett.* **77**, 135 (1996).
- [5] R.D. Tscheuschner and A.D. Wieck, *Superlattices and Microstructures* **20**, 615 (1996).
- [6] A. Kristensen, J.B. Jensen, M. Zaffalon, C.B. Sørensen, S.M. Reimann, P.E. Lindelof, M. Michel, and A. Forchel, *J. Appl. Phys.* **83**, 607 (1998).
- [7] A. Kristensen, P.E. Lindelof, J.B. Jensen, M. Zaffalon, J. Hollingbery, S.W. Pedersen, J. Nygård, H. Bruus, S.M. Reimann, C.B. Sørensen, M. Michel, and A. Forchel, *Physica B* **249-251**, 180 (1998).
- [8] B.E. Kane, G.R. Facer, A.S. Dzurak, N.E. Lumpkin, R.G. Clark, L.N. Pfeiffer, and K.W. West, *Appl. Phys. Lett.* **72**, 3506 (1998).
- [9] K.J. Thomas, J.T. Nicholls, M. Pepper, W.R. Tribe, M.Y. Simmons, and D.A. Ritchie, *Phys. Rev. B* **61**, R13365 (2000).
- [10] A. Kristensen, H. Bruus, A. Forchel, J.B. Jensen, P.E. Lindelof, M. Michel, J. Nygård, and C.B. Sørensen, *Phys. Rev. B* **62**, 10950 (2000).
- [11] K.S. Pyshkin, C.J.B. Ford, R.H. Harell, M. Pepper, E.H. Linfield, and D.A. Ritchie, *Phys. Rev. B* **62**, 15842 (2000).
- [12] S. Nuttinck, K. Hashimoto, S. Miyashita, T. Saku, Y. Yamamoto, and Y. Hirayama. *Jpn. J. Appl. Phys.* **39**, L655 (2000).
- [13] K. Hashimoto, S. Miyashita, T. Saku, and Y. Hirayama *Jpn. J. Appl. Phys.* **40**, 3000 (2001).
- [14] D. J. Reilly, G. R. Facer, A. S. Dzurak, B. E. Kane, R. G. Clark, P. J. Stiles, J. L. O'Brien, N. E. Lumpkin, L. N. Pfeiffer, K. W. West, *Phys. Rev. B* **63**, R121311 (2001).
- [15] K.J. Thomas, J.T. Nicholls, M.Y. Simmons, M. Pepper, D.R. Mace, and D.A. Ritchie, *Phil. Mag.* **77**, 1213 (1998)
- [16] K.J. Thomas, J.T. Nicholls, N.J. Appleyard, M. Pepper, M.Y. Simmons, D.R. Mace, W.R. Tribe and D.A. Ritchie, *Phys. Rev. B* **58**, 4846 (1998).
- [17] C.-T. Liang, M.Y. Simmons, C.G. Smith, G.H. Kim, D.A. Ritchie and M. Pepper, *Phys. Rev. B* **60**, 10687 (1999).
- [18] T.G. Griffiths, E. Comforti, M. Heiblum, and V. Umansky, *ICPS-25 workbook*, 316 (2000).
- [19] N. J. Appleyard, J. T. Nicholls, M. Pepper, W. R. Tribe, M. Y. Simmons, and D. A. Ritchie, *Phys. Rev. B* **62**, R16275 (2000).
- [20] J. Cunningham, V.I. Talyanskii, J.M. Shilton, M. Pepper, A. Kristensen, and P.E. Lindelof, to be published (2001).
- [21] H. Bruus, V.V. Cheianov, and K. Flensberg, *Physica E* **10**, 97-102 (2001).
- [22] N.K. Patel, J.T. Nicholls, L. Martin-Moreno, M. Pepper, J.E.F. Frost, D.A. Ritchie and G.A.C. Jones *Phys. Rev. B* **44**, 13549 (1991).
- [23] L.I. Glazman and A. V. Khaetskii, *Europhys. Lett.* **9**, 263 (1989).
- [24] M. Büttiker, *Phys. Rev B* **41**, 7906 (1990)
- [25] H. Bruus, V.V. Cheianov, and K. Flensberg, *Proc. XXXVI Rencontres de Moriond* (in press, 2001).